



MODELING AND SIMULATION OF A VIBRATING MICROCANTILEVER BEAM IN ATOMIC FORCE MICROSCOPES

Kleber dos Santos Rodrigues

Marcelo Areias Trindade

São Carlos School of Engineering, University of São Paulo, Av. Trabalhador São Carlense, 400, 13566-590, São Carlos SP, Brazil
ksrodrigues@usp.br, trindade@sc.usp.br

Abstract. *The Atomic Force Microscope (AFM) is an indispensable tool in Scanning Probe Microscopy. In its core, a moving microcantilever beam with a sharp probing tip is used to scan a sample surface. As a result of the atomic-level interactions between the probing tip and the sample surface to be analysed, the microcantilever beam is deflected. The deflections of the microcantilever beam tip are detected by a photo detector through the reflection of a laser beam. The magnitude of the attractive/repulsive interaction forces lies within the range of nano and pico Newtons and, thus, very precise information may be obtained on the topography of the sample surface. The transversal motion of the microcantilever beam is controlled by a piezoelectric actuator placed at its base, while the another xyz piezoelectric actuator is responsible for the displacement of the sample. Since the interaction forces between probe tip and sample are highly nonlinear, their modeling and understanding are very important for the design of the microcantilever beam and effective control law. This work aims to present a numerical model of a typical AFM microcantilever beam and an analysis of its response when subjected simultaneously to a controlled actuation at its base and to interaction forces at its tip. In this preliminary study, the base actuation is considered to be a known harmonic displacement, as in tapping or non-contact AFM operation mode, while the interactions forces are modeled as van der Waals forces. The microcantilever beam is modeled using a sliding-free beam finite element model with concentrated inertia at its tip. The effect of damping properties and interaction force parameters on the resulting motion for a number of sample surfaces situations is analysed through numerical simulations.*

Keywords: *Atomic force microscopy, Microcantilever Beams, van der Waals, Interaction Forces, Nonlinear dynamics*

1. INTRODUCTION

The Atomic Force Microscope (AFM) represents one of the most powerful tools in Scanning Probe Microscopy (SPM) (Binnig *et al.*, 1986; Meyer, 1992). In the core of the device, a microcantilever drive a probe with a sharp tip over the sample surface. An optical system (composed by a laser and a photo detector) detects the microcantilever deflections. A feedback control system is responsible to keep constant the distance/force between tip set point and sample.

Three modes of operation are the most commonly used in AFM: contact, intermittent (tapping) and non-contact mode. In contact mode, the probe tip is dragged over the sample surface and the actuating forces are predominantly repulsive. The deflection of microcantilever is then function of the interaction forces between probe tip and sample. In non-contact mode, the probe tip is kept at a larger distance from the sample to avoid tip or sample degradation and friction related problems. However, in this case, the interaction forces are also smaller and thus less sensitive to the sample topography. In tapping mode, the microcantilever is excited by a harmonic excitation at its base so that the probe tip can be closer to the sample leading to better sensitivity while avoiding or minimizing the issue of tip-sample sticking (of non-contact mode) and tip or sample degradation (of contact mode). The microcantilever is normally excited near its resonance frequency and the deflection amplitude of the probe tip is function of the interaction forces between probe tip and sample (Binnig *et al.*, 1986; Meyer, 1992).

The intermolecular interaction forces between probe tip and sample surface are due specifically to the fluctuations of electrons in molecules. These interactions are present in molecules polar permanent and are generally the largest contribution to this forces (Israelachvili, 1991). With an AFM device, it is possible to measure the very small interaction forces acting between probe tip and sample. At very short distances ($< 5\text{Å}$), the actuating forces are inherently repulsive (Pauli principle) while, for distances between $5 - 10\text{Å}$, the contributions comes instead from attractive van der Waals forces.

The complexity of the AFM operation system became an interesting issue in the scientific community, and the use of mathematical modelling became indispensable for understanding the dynamics and designing more effective control strategies for the system (Jalili and Laxminarayana, 2004). The literature presents the predominance of discrete models to represent the probe tip/sample interactions. Mathematical models presented in (Dankowicz, 2006; Misra *et al.*, 2008; Nozaki *et al.*, 2010; Balthazar *et al.*, 2012; Zhao and Dankowicz, 2006; Rodrigues *et al.*, 2011) and others assume that the stiffness of the microcantilever may be represented by a spring element and, thus, a one degree-of-freedom system is considered as composed by a lumped mass (mass of probe tip), lumped damper (representing all sources of damping such as air or liquid viscous damping) and lumped spring (linear and/or non-linear) and subjected to a point force applied to

the lumped mass (representing the tip-sample interaction force) and a prescribed base displacement or force (representing the base excitation).

According to (Fang *et al.*, 2002b), this simplified approach neglects the distributed beam effects as well as the shear force component at the tip. In (Stark *et al.*, 2004) and (Rutzel *et al.*, 2003), the authors used continuum models to represent the microcantilever dynamics. In (Howard-Knight and Hobbs, 2011), a dynamic finite element model has been constructed to simulate the behavior of low spring constant atomic force microscope (AFM). In (Fang *et al.*, 2002a), analytical solutions to a complex dynamic system were achieved via finite element method. In (Babahosseini *et al.*, 2009), a finite element model is used and applied to the design of a sliding mode controller. The system is represented by a sliding-free Euler-Bernoulli beam with lumped mass at its free end where van der Waals forces are considered. For the base excitation, both prescribed displacement and imposed force are considered and numerical simulations with same parameters show significant differences between the two methods. The system was also shown to be sensitive to variations in damping coefficients.

This work aims to present a numerical model of a typical AFM microcantilever beam and an analysis of its response when subjected simultaneously to a controlled actuation at its base and to interaction forces at its tip. Both prescribed displacement and force are considered for the base excitation and van der Waals forces are considered for the interaction between beam tip and sample surface. The microcantilever beam is modeled using a sliding-free beam finite element model with concentrated inertia at its tip.

2. FINITE ELEMENT MODELING OF THE AFM MICROCANTILEVER BEAM

A standard Bernoulli-Euler beam finite element model was considered to model the AFM microcantilever beam. The beam is considered to be homogeneous and uniform with length L , width b , thickness h and made of a material with Young's modulus E , Poisson's ratio ν and mass density ρ . As shown in Figure 1, a concentrated inertia, with mass m_t and moment of inertia I_t , is included at the free end (tip) of the beam where the beam is also subjected to a concentrated attractive van der Waals force f_t . The probe tip is initially set at a distance d from the sample surface.

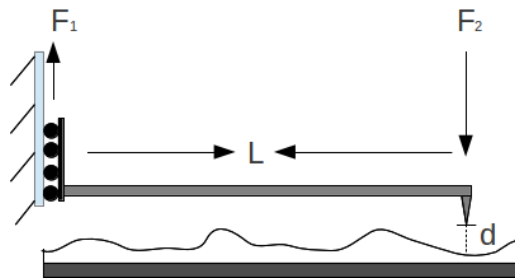


Figure 1. Schematic representation of the AFM microcantilever beam.

2.1 Finite element discretization of displacements and strains

Considering the standard Bernoulli-Euler hypothesis for a slender beam in xz plane deflection, the displacements field can be written as

$$\bar{u}(x,y,z,t) = -zw'(x,t), \quad \bar{v}(x,y,z,t) = 0, \quad \bar{w}(x,y,z,t) = w(x,t), \quad (1)$$

where $w' = \partial w / \partial x$ is the cross-section rotation angle.

Based on these kinematic hypotheses, the only non-null mechanical strain, that is the normal longitudinal strain ε_x , can be written from the usual strain-displacement relation as

$$\varepsilon_x = -zw''. \quad (2)$$

Hermite cubic shape functions are assumed for the discretization of the transverse deflection $w(x,t)$, along the element length L_e , such that a two node finite element with two degrees of freedom per node, namely deflection w_i and cross-section rotation angle w'_i ($i = 1, 2$), is obtained as shown in Figure 2.

The elementary degrees of freedom (dof) column vector \mathbf{u}_e is defined as

$$\mathbf{u}_e = \begin{bmatrix} w_1 \\ w'_1 \\ w_2 \\ w'_2 \end{bmatrix}, \quad (3)$$



Figure 2. Bernoulli-Euler beam finite element.

and the transverse displacement of the cantilever can be written in terms of the elementary dofs as

$$w(x,t) = \mathbf{N}(x)\mathbf{u}_e(t), \quad (4)$$

where

$$\begin{aligned} \mathbf{N}(x) &= [N_1(x) \quad N_2(x) \quad N_3(x) \quad N_4(x)], \\ N_1(x) &= \frac{1}{2} - \frac{3}{2L_e}x + \frac{2}{L_e^3}x^3, \\ N_2(x) &= \frac{L_e}{8} - \frac{1}{4}x + \frac{1}{2L_e}x^2 + \frac{1}{L_e}x^3, \\ N_3(x) &= \frac{1}{2} - \frac{3}{2L_e}x - \frac{2}{L_e^3}x^3, \\ N_4(x) &= -\frac{L_e}{8} - \frac{1}{4}x + \frac{1}{2L_e}x^2 + \frac{1}{L_e}x^3. \end{aligned} \quad (5)$$

Using (2), the normal strains can be discretized and written in terms of the elementary dof as

$$\varepsilon_x = -z\mathbf{B}\mathbf{u}_e, \text{ with } \mathbf{B} = \mathbf{N}''. \quad (6)$$

2.2 Variational formulation

The equation of motions can be written using Hamilton's principle

$$\delta\Pi = \int (\delta T - \delta V + \delta W) dt \quad (7)$$

where δT and δV are the virtual variations of the kinetic and potential energy and δW is the virtual work done by applied mechanical forces.

The virtual variation of kinetic energy can be written using the displacements fields defined in (1), such that

$$\int \delta T dt = - \int \int_{\Omega} \delta w \rho \ddot{w} d\Omega dt. \quad (8)$$

Since neither w nor ρ depend on the position in the cross-section yz , the integral over the beam volume can be directly rewritten as the following integral over length x

$$\int \delta T dt = - \int_0^{L_e} \delta w \rho A \ddot{w} dx dt. \quad (9)$$

Replacing the transverse displacement w by its discretized counterpart, defined in (4), yields

$$\int \delta T dt = - \int \delta \mathbf{u}_e^t \mathbf{M}_e \ddot{\mathbf{u}}_e dt, \quad (10)$$

where \mathbf{M}_e is the elementary mass matrix of the beam, defined as

$$\mathbf{M}_e = \int_0^{L_e} \rho A \mathbf{N}^t \mathbf{N} dx. \quad (11)$$

The virtual variation of the potential energy is written in terms of the deformation energy of an elementary volume of the beam as

$$\delta V = \int_{\Omega} \delta \varepsilon_x \sigma_x d\Omega, \quad (12)$$

where σ_x is the longitudinal normal stress which, considering a linear elastic material with Young's modulus E for the microcantilever beam, can be written as

$$\sigma_x = E \varepsilon_x. \quad (13)$$

Substitution of (13) in (12) results

$$\delta V = \int_{\Omega} \delta \varepsilon_x E \varepsilon_x d\Omega, \quad (14)$$

which can be written in terms of the elementary dof vector \mathbf{u}_e , using (6) and integrating over the cross-section area, as

$$\delta V = \delta \mathbf{u}_e^t \mathbf{K}_e \mathbf{u}_e, \quad (15)$$

where \mathbf{K}_e is the stiffness matrix of the element, defined as

$$\mathbf{K}_e = \int_0^{L_e} E I \mathbf{B}^t \mathbf{B} dx. \quad (16)$$

The second moment of area I of the beam cross-section is

$$I = \int_A z^2 dA. \quad (17)$$

Notice that, in both (11) and (16), the material and geometrical properties of the beam, ρ , E , A and I , may be variable along beam's length and, thus, functions of x .

For simplicity, the virtual work done by applied mechanical forces is constructed directly from a known vector of nodal forces \mathbf{F} , such that

$$\delta W = \delta \mathbf{u}_e^t \mathbf{F}. \quad (18)$$

2.3 Equations of motion for the AFM microcantilever accounting for the probe tip

In addition to the variational quantities of the microcantilever beam, the probe tip is considered as a lumped inertia concentrated at the node located at the free end of the beam. Both mass m_t and moment of inertia I_t , with respect to the tip node, of the probe tip are accounted for. This is done by including two additional kinetic energy terms corresponding to the translational kinetic energy, written in terms of deflection $w(L, t)$ at the tip, and rotational kinetic energy, written in terms of cross-section rotation $w'(L, t)$.

Hence, using equations (10), (15) and (18), summing for all finite elements and including the kinetic energy variations related to the probe tip, the extended Hamilton's principle is rewritten as

$$\delta \Pi = \int \left\{ \delta \mathbf{u}^t (\mathbf{M} \ddot{\mathbf{u}} + \mathbf{D} \dot{\mathbf{u}} + \mathbf{K} \mathbf{u} - \mathbf{F}) + [\delta w(L, t) m_t \ddot{w}(L, t) + \delta w'(L, t) I_t \ddot{w}'(L, t)] \right\} dt = 0, \quad (19)$$

where \mathbf{u} is the global dof vector, \mathbf{M} , \mathbf{D} and \mathbf{K} are global mass, damping and stiffness matrices and \mathbf{F} is the global applied forces vector.

Notice that both the deflection and cross-section rotation angle at the beam tip, $w(L, t)$ and $w'(L, t)$, are included in the global dof vector \mathbf{u} and, thus,

$$w(L, t) = \mathbf{L}_w \mathbf{u}, \quad w'(L, t) = \mathbf{L}_{w'} \mathbf{u}, \quad (20)$$

with

$$\mathbf{L}_w = [0 \quad \cdots \quad 0 \quad 1 \quad 0], \quad \mathbf{L}_{wx} = [0 \quad \cdots \quad 0 \quad 1]. \quad (21)$$

Replacing (20) in (19) leads to

$$(\mathbf{M} + \mathbf{M}_t)\ddot{\mathbf{u}} + \mathbf{D}\dot{\mathbf{u}} + \mathbf{K}\mathbf{u} = \mathbf{F}, \quad (22)$$

where the equivalent mass matrix corresponding to the probe tip, \mathbf{M}_t , is written as

$$\mathbf{M}_t = \mathbf{L}_w^t m_t \mathbf{L}_w + \mathbf{L}_{wx}^t I \mathbf{L}_{wx}. \quad (23)$$

The ad-hoc damping matrix \mathbf{D} included in the equations of motion was considered to be proportional to the microcantilever mass and stiffness matrices, \mathbf{M} and \mathbf{K} , such that

$$\mathbf{D} = \alpha \mathbf{M} + \beta \mathbf{K}, \quad (24)$$

where the constants α and β must be determined a posteriori.

3. BOUNDARY CONDITIONS

The base excitation and tip-sample interaction forces are implemented as boundary conditions at the base ($x = 0$) and at the free end ($x = L$), respectively, in the finite element model presented previously. For the base excitation, two methods are considered: prescribed displacement and imposed force. For the tip-sample interaction forces, attractive van der Waals forces are considered.

3.1 Interactions forces between probe tip and sample surface

In the present work, only van der Waals attractive forces between probe tip and sample surface are considered. This should be a reasonable approximation as long as the distance between probe tip and sample surface remains larger than 5\AA . An expression describing the behavior of these interaction forces between two spherical bodies with smooth surfaces was developed by Hamaker (Israelachvili, 1991), in terms of the radii of the two spherical bodies, the distance between them and a constant, so-called Hamaker coefficient, that depends on the material properties of the two bodies.

Supposing that the sample surface could be considered as a spherical body with radius much larger than the one of the probe tip and that the distance between the probe tip and sample surface is much smaller than the probe tip radius, the general expression developed by Hamaker can be simplified to

$$f_t = -\frac{HR}{6r^2} \quad (25)$$

where H is the Hamaker constant, R is the probe tip radius and r is the distance between probe tip and sample surface. The Hamaker constant may be written as $H = \pi^2 C \rho_1 \rho_2$, where ρ_1 and ρ_2 are the number of atoms per unit volume in the each body and C is the interaction coefficient of particle-particle intermolecular potential (Rutzel *et al.*, 2003). Thus, for known probe tip, the Hamaker constant may vary depending on the material properties of the sample surface. Therefore, the van der Waals force should be sensitive for changes not only in the distance between probe tip and sample surface (sample surface topography) but also in the material properties of the sample surface.

In the present case, the probe tip may vary dynamically due to the deflection of the microcantilever and, thus, the distance between probe tip and sample surface is written as

$$r(t) = d + w(L, t), \quad (26)$$

where d is the initial distance, that is for undeformed microcantilever beam, named set point distance, and $w(L, t)$ is the deflection of the microcantilever beam free end, considered to be equal to the transversal displacement of the probe tip.

Replacing (26) in (25) leads to

$$f_t(t) = -\frac{HR}{6[d + w(L, t)]^2}. \quad (27)$$

In order to include the van der Waals force into the finite element model, a force vector $\mathbf{F}_t(t) = \mathbf{b}_t f_t(t)$ is defined, where $\mathbf{b}_t = [0 \cdots 0 \quad 1 \quad 0]$ is a boolean vector that associates the force amplitude $f_t(t)$ with the nodal dof corresponding to the transverse displacement at the free end of the microcantilever beam. This force vector is then included as an applied mechanical forces vector in equation (22).

K.S. Rodrigues and M.A. Trindade
Modeling and Simulation of a Vibrating Microncantilever Beam in AFM

3.2 Base excitation of AFM microcantilever beam

At the other extremity ($x = 0$), the microcantilever beam is supposed to be clamped to a moving base in transversal displacement only, so that the beam cross-section rotation angle at this point is set to zero, that is $w'(0, t) = 0$. Then, two different approaches were used to account for the transversal motion of the moving base by considering at $x = 0$: either an imposed force $f_b(t)$ applied by the moving base to the microcantilever beam or a prescribed displacement $w(0, t) = z(t)$ of the microcantilever beam.

In the case of imposed transversal force at the base of the microcantilever beam, a force vector $\mathbf{F}_b(t) = \mathbf{b}_b f_b(t)$ is defined, where $\mathbf{b}_b = [1 \ 0 \ \dots \ 0]$ is a boolean vector that associates the force amplitude $f_b(t)$ with the nodal dof corresponding to the transverse displacement at the base end of the microcantilever beam. This force vector is then included as an applied mechanical forces vector in equation (22).

In the present work, a known sinusoidal excitation force is considered, such that $f_b(t) = \tilde{f}_b \sin(\omega_b t)$. The excitation amplitude and frequency are defined in the next section.

In the case of prescribed displacement, the finite element model dof corresponding to the transversal displacement at the base end is separated from the others, so that the equations of motion (22) are rewritten as

$$[\delta w_1 \quad \delta \mathbf{u}_r^t] \left\{ \begin{bmatrix} M_{pp} & \mathbf{M}_{pr} \\ \mathbf{M}_{pr}^t & \mathbf{M}_{rr} \end{bmatrix} \begin{bmatrix} \dot{w}_1 \\ \dot{\mathbf{u}}_r \end{bmatrix} + \begin{bmatrix} D_{pp} & \mathbf{D}_{pr} \\ \mathbf{D}_{pr}^t & \mathbf{D}_{rr} \end{bmatrix} \begin{bmatrix} \dot{w}_1 \\ \dot{\mathbf{u}}_r \end{bmatrix} + \begin{bmatrix} K_{pp} & \mathbf{K}_{pr} \\ \mathbf{K}_{pr}^t & \mathbf{K}_{rr} \end{bmatrix} \begin{bmatrix} w_1 \\ \mathbf{u}_r \end{bmatrix} - \begin{bmatrix} f_p \\ \mathbf{F}_r \end{bmatrix} \right\} = 0, \quad (28)$$

where $w_1(t)$ is the prescribed displacement at the base end of the microcantilever beam and \mathbf{u}_r is the remaining unknown dofs vector. Then, considering that $\delta w_1 = 0$, since w_1 is prescribed, the first line of (28) is automatically solved and the terms involving w_1 can be included as an equivalent force applied to the remaining system

$$\mathbf{M}_{rr} \ddot{\mathbf{u}}_r + \mathbf{D}_{rr} \dot{\mathbf{u}}_r + \mathbf{K}_{rr} \mathbf{u}_r = \mathbf{F}_r + \mathbf{F}_p, \quad (29)$$

where the equivalent force vector \mathbf{F}_p associated with the prescribed base displacement is written as

$$\mathbf{F}_p = \mathbf{M}_{pr}^t \ddot{w}_1 + \mathbf{D}_{pr}^t \dot{w}_1 + \mathbf{K}_{pr}^t w_1 \quad (30)$$

If a known sinusoidal base transversal displacement is considered, such that $w_1(t) = \tilde{w}_1 \sin(\omega_b t)$, the corresponding force vector \mathbf{F}_p is

$$\mathbf{F}_p = [(-\omega_b^2 \mathbf{M}_{pr}^t + \mathbf{K}_{pr}^t) \sin(\omega_b t) + \omega_b \mathbf{D}_{pr}^t \cos(\omega_b t)] \tilde{w}_1. \quad (31)$$

The prescribed displacement amplitude \tilde{w}_1 and frequency ω_b are defined in the next section.

4. NUMERICAL SIMULATIONS AND RESULTS

This section presents some initial simulations obtained with the proposed models. The parameters used are in table 1. It corresponds to the interactions of a particle coated with a gold layer on the silicon oxide substrate, the afm tip is composed by silicon (Babahosseini *et al.* (2009)) :

Table 1. Parameters

Parameter	Symbol	Value	Unit
Length of microcantilever	L	449×10^{-6}	m
Width of the microcantilever	W	46×10^{-6}	m
Thickness of the microcantilever	T	1.7×10^{-6}	m
Young Modulus	E	176×10^9	N/m^2
Microcantilever density	ρ	2330	Kg/m^3
Moment of inertia	I	1.8×10^{-23}	m^4
Area	A	7.8×10^{-11}	m^2
Tip radius	R	150×10^{-9}	m
Hammaker constant	H	1.865×10^{-19}	J
Tip mass	M_t	3×10^{-10}	Kg
Tip moment of inertia	I_{M_t}	23.4×10^{-22}	Kg/m^3
Excitation Frequency	ω_b	9×10^3	Hz
Tip-sample distance	d	7.5×10^{-9}	m
Excitation amplitude	\hat{f}_b	2×10^{10}	N
Presc. displacement amplitude	\tilde{w}_1	4×10^{-9}	m

The next table presents de five first natural frequencies of the microcantilever calculated considering prescribed displacement and imposed force.

Table 2. Natural frequencies (kHz)

f_n	Imposed Force	Prescribed Displacement
f_1	9.1	2.9
f_2	75.4	52.6
f_3	206.7	167.9
f_4	400.4	346.3
f_5	651.6	583.8

As seem in table 2, from third natural frequency, the values increase rapidly, it complicates the analysis of the system responses. The presence of these high frequency complicates the analysis of obtained data, in addition to significantly increasing the computational cost. To solve this problem, a transformation to the modal base was realized with a modal reduction. Next sections presents the modal reduction of the system to a new system with 3 degrees of freedom.

4.1 Modal reduction of the system

By equation (22) and assuming $(\mathbf{M} + \mathbf{M}_t) = \mathbf{M}_T$, the system without damping and free of external forces may written as:

$$\mathbf{M}_T \ddot{\mathbf{u}} + \mathbf{K} \mathbf{u} = 0, \quad (32)$$

and the solution is:

$$\mathbf{u} = \phi e^{\lambda t} \quad (33)$$

Using (33) in (32), results in a system that can be written as:

$$(\lambda^2 \mathbf{M}_T + \mathbf{K}) \phi^{\lambda t} = 0 \quad (34)$$

The result of $\det(\lambda^2 \mathbf{M}_T + \mathbf{K}) = 0$ gives

$$\lambda_r = i\omega_r, \quad (35)$$

K.S. Rodrigues and M.A. Trindade
Modeling and Simulation of a Vibrating Microncantilever Beam in AFM

and ω_r is the r -th natural frequency. Substitution of (35) in (34) result in an eigenvector ϕ_r that corresponds to the r -th vibration mode of system. Considering Φ as a $N \times N$ matrix of the vibration modes ϕ_{ij} , is possible to obtain a modal coordinate \mathbf{q} , as a function of nodal coordinates \mathbf{u} :

$$\mathbf{u} = \Phi \mathbf{q} \quad (36)$$

The new equation of motion is:

$$\Phi^T \mathbf{M}_T \Phi \ddot{\mathbf{q}} + \Phi^T \mathbf{D} \Phi \dot{\mathbf{q}} + \Phi^T \mathbf{K} \Phi \mathbf{q} = \Phi^T \mathbf{F}_T, \quad (37)$$

Where:

$$\Phi^T \mathbf{M} \Phi = I, \quad (38)$$

is an identity matrix.

$$\Phi \mathbf{K} \Phi = \Omega^2 \quad (39)$$

the $\sqrt{\Omega^2}$ is a diagonal matrix with the natural frequencies ω_n .

$$\Phi^T \mathbf{D} \Phi = \Lambda, \quad (40)$$

Λ is a diagonal matrix where the elements are $2\zeta_n \omega_n$.

Lastly,

$$\Phi^T \mathbf{F}_T = \mathbf{F}_{Mod}, \quad (41)$$

where \mathbf{F}_{Mod} is a column force matrix with the contributions of the vibration modes.

In the modal reduced base, considering three vibration mode, the system may be written as:

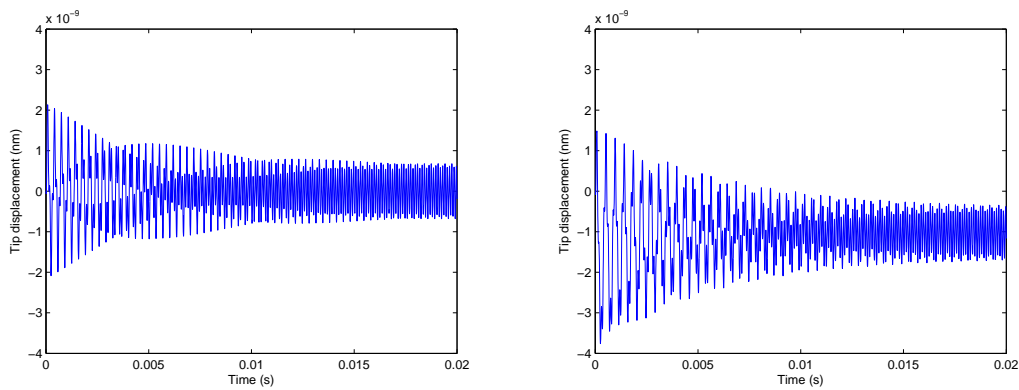
$$\ddot{\mathbf{q}} + \Lambda \dot{\mathbf{q}} + \Omega^2 \mathbf{q} = \mathbf{F}_{mod} \quad (42)$$

4.2 Comparison between the results with prescribed displacement and force imposed

The aim of this section is the comparison of the systems with and without the influence of the Van der Waals forces through time history, phase portraits and Fft analysis. For both systems, the adopted damping parameter is $\alpha = \beta = 1 \times 10^{-6}$. For the simulations, 30 beam finite elements was chosen.

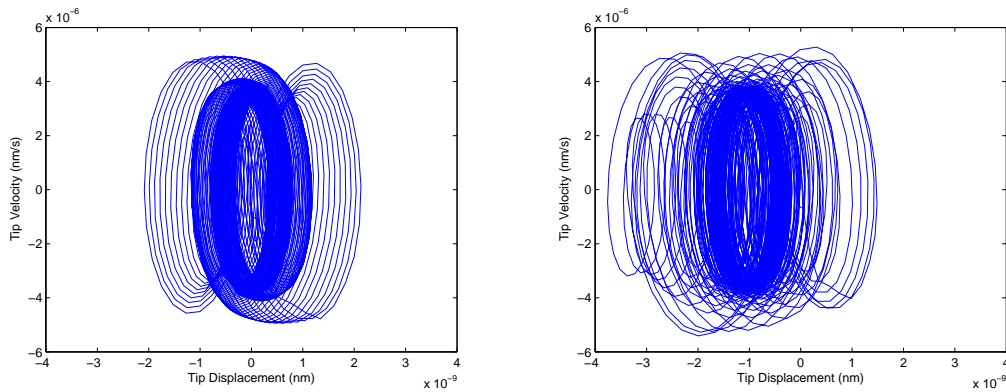
a) Prescribed displacement:

This section presents the results of simulation of the system with prescribed displacement. For the system without the influence of the Van der Waals forces, it is possible to observe the beating phenomenon, and the displacement amplitude is proportional along the time axis. In the presence of Van der Waals forces, the system shows predominantly negative displacements at the tip, without beating phenomenon.



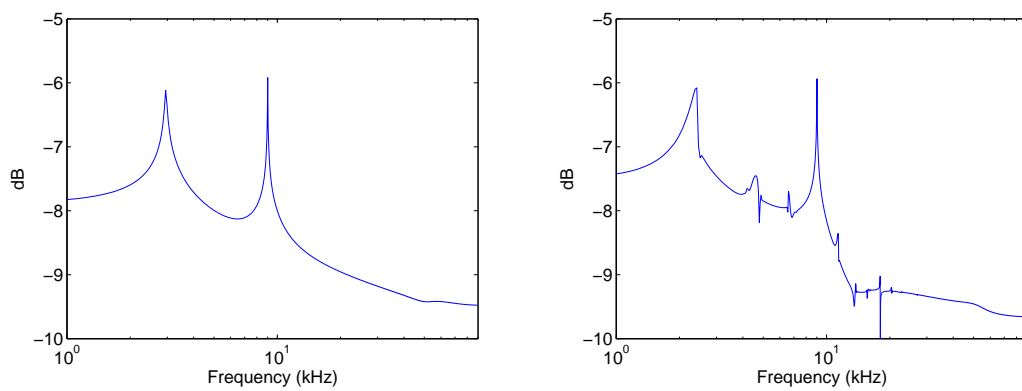
(a) Tip displacement without Van der Walls (b) Tip displacement with Van der Walls
Figure 3. (a):Tip displacement without Van der Walls, (b):Tip displacement with Van der Waals

The phase portraits confirms the time history analysis, in 7(a) and 7(b) the velocities have the same magnitude, but the displacements in 7(b) are shifted to the left (negative region) showing a system with irregular behavior.



(a) Phase portrait without Van der Walls (b) Phase portrait with Van de Walls
Figure 4. (a): Phase portrait without Van der Walls, (b): Phase portrait with Van der Walls

Without the presence Van der Waals, the fft presents peaks in the first natural and in the excitation frequency. With the presence of Van der Walls, new peaks appears, including peaks multiples of $9kHz$, phenomenon that reveals the nonlinearities emerged by the actuation of Van der Walls forces.



(a) Fft without Van der Walls (b) Fft with Van der Walls
Figure 5. (a): Fft with Van der Walls, (b): Fft without Van der Walls

b) Imposed Force:

For the imposed force approach, the beating phenomenon appears due to the proximity between the natural and excitation frequencies.

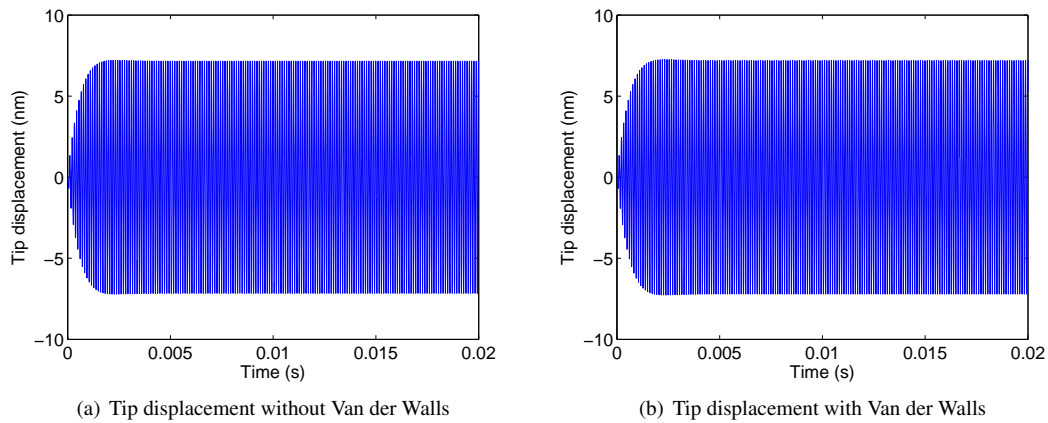


Figure 6. (a):Tip displacement without Van der Waals, (b):Tip displacement with Van der Waals

The phase portraits in 7(a) and 7(b) shows a periodic behavior even with the presence of Van der Waals.

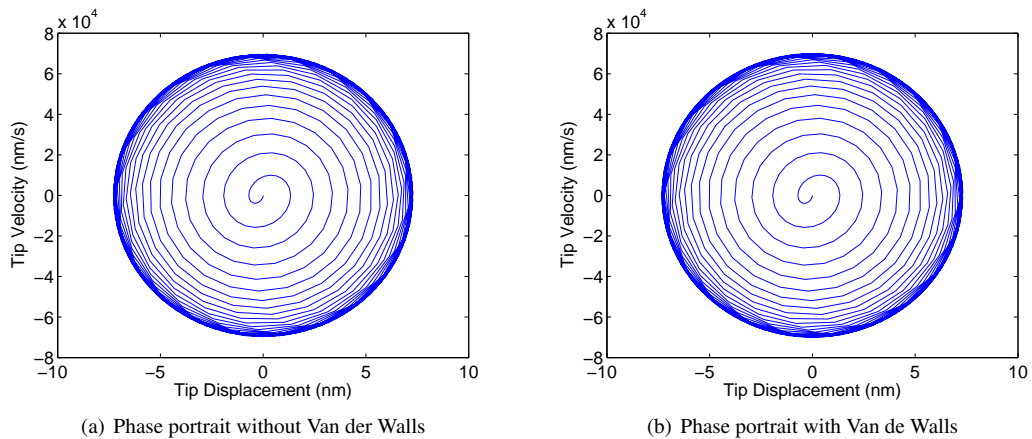


Figure 7. (a): Phase portrait without Van der Waals, (b): Phase portrait with Van der Waals

The Fft analysis shows only the excitation peak and a small one that is a multiple of the first, representing a nonlinearity occurred by the presence of Van der Waals forces

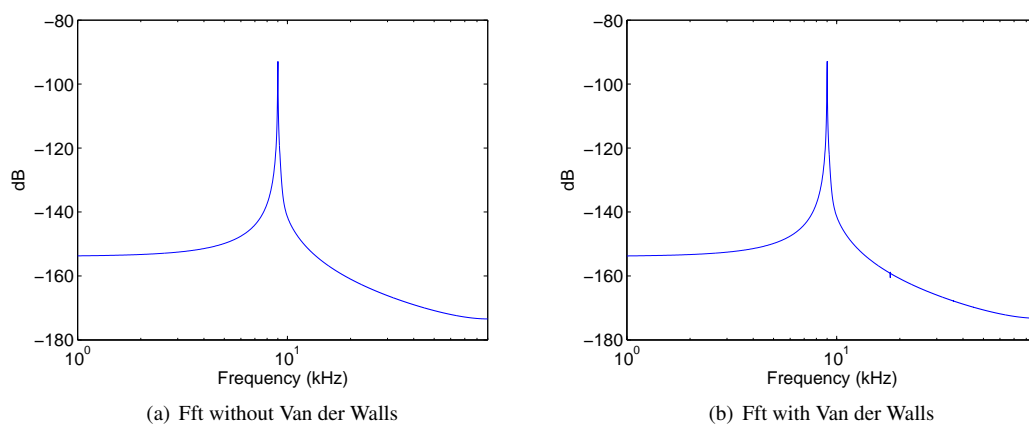


Figure 8. (a): Fft with Van der Waals, (b): Fft without Van der Waals

With the adopted parameters, a comparison between the system with imposed force and prescribed displacement may be realized. With prescribed displacement, a strong presence of transient regime can be observed, it happens because the signal adopted to excite the system have a strong actuation when the movement begins, after a certain time interval, it starts the permanent regime and stay stabilized. For the imposed force, the presence of Van der Waals forces are very softly. Next section, shows the simulations of the system with different values for the damping

coefficients α and β .

4.3 Variation of damping coefficients

This section presents the results with the increasing of the damping coefficients, with values $\alpha = \beta = 1 \times 10^{-5}$ and $\alpha = \beta = 1 \times 10^{-4}$

a) System with prescribed displacement:

In the figures 10(b) and 9(b), the increase of damping effect minimizes the transient region, and leaves the steady dominate the dynamics of the system.

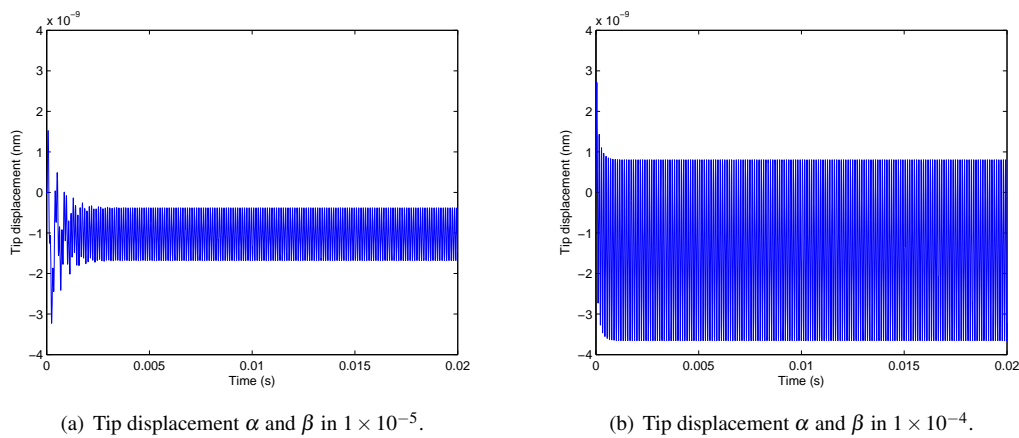


Figure 9. Tip displacement with variation of damping coefficients.

In the FFT, the increased damping reduces the presence of the resonance peaks, leaving only the multiple peaks of the excitation frequency, emphasizing the non-linearity of the Van der Waals forces

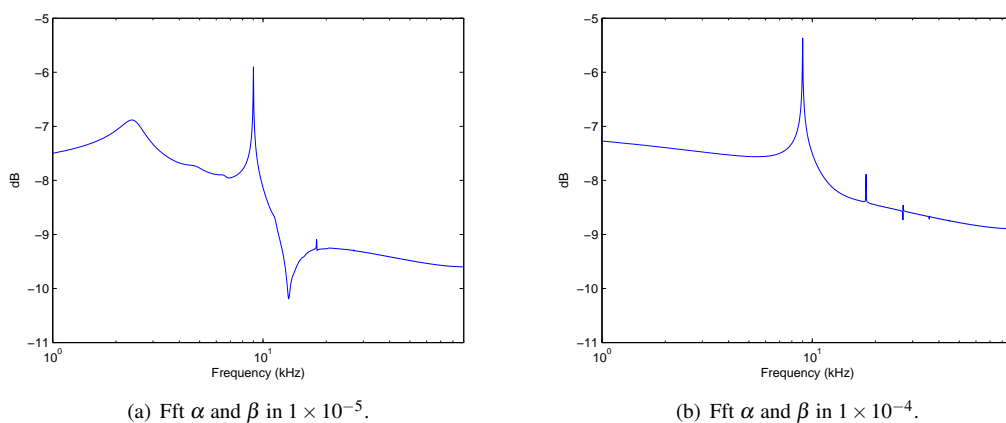


Figure 10. Fft with variation of damping coefficients.

b) Imposed force:

On the force imposed system, as damping increases, there is a considerable decrease in the amplitude of displacement of the tip.

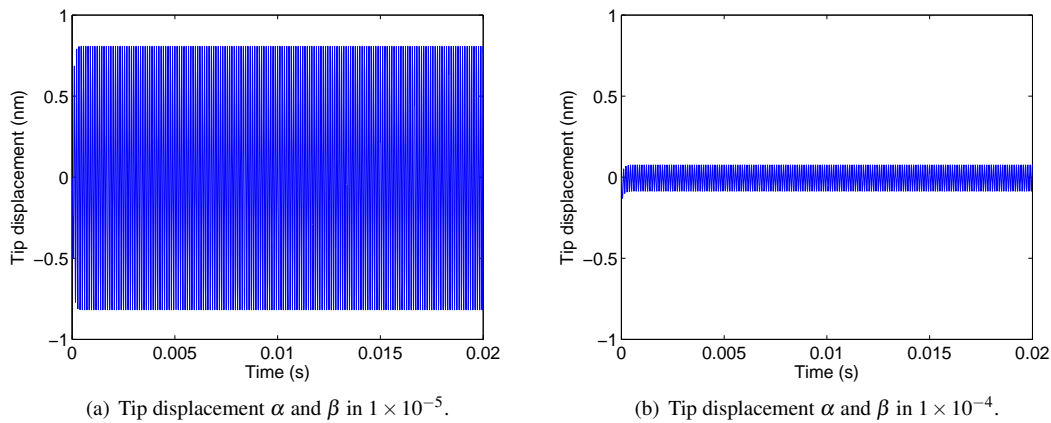


Figure 11. Tip displacement with variation of damping coefficients.

In the fft analysis, there is a reduction in the size of the peak, as well as an attenuation of the effect of Van der Waals forces.

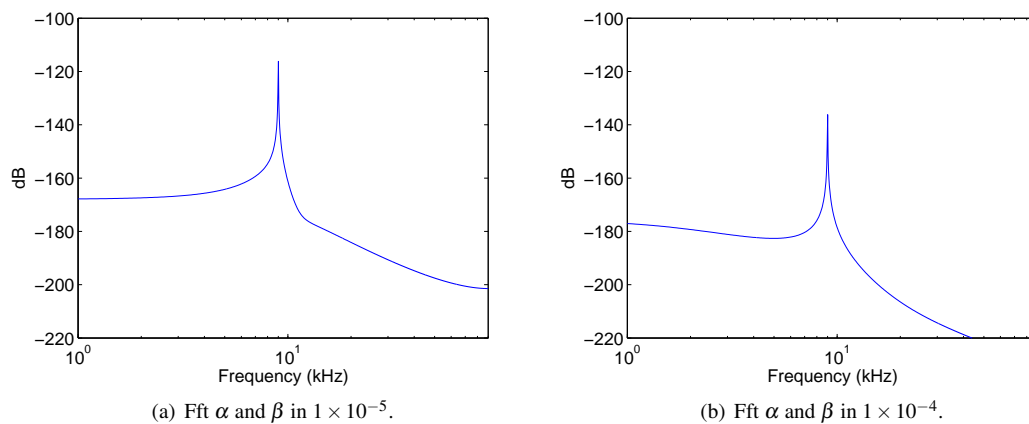


Figure 12. Fft with variation of damping coefficients.

The comparison between both systems shows a different actuation of the damping effects. In the system with prescribed displacement, the effect regulates the displacement of the tip, taking the high amplitude transient. To the imposed force approach, it greatly decreases this displacement, an effect that may provide no benefit to the operation of the system, since the vibration amplitude in non-contact mode ranges from 1 to 10nm.

5. CONCLUSIONS

This work presented a numerical model of a typical AFM microcantilever beam and an analysis of its response when subjected simultaneously to a controlled actuation at its base and to interaction forces at its tip. The base actuation was considered to be a known harmonic displacement, while the interactions forces were modeled as van der Waals forces. The microcantilever beam was modeled using a sliding-free beam finite element model with concentrated inertia at its tip. The effect of base excitation approach, damping properties and interaction force parameters on the resulting motion were analysed through numerical simulations. Future works will be directed to the inclusion of other approaches for modeling the interaction forces between probe tip and sample surface, for instance Derjaguin-Muller-Toporov (DMT) model and Lennard-Jones potential.

6. ACKNOWLEDGEMENTS

Support of MCT/CNPq/FAPEMIG National Institute of Science and Technology on Smart Structures in Engineering, grant 574001/2008-5, is acknowledged. The first author acknowledges also the support of CAPES for a doctoral scholarship.

7. REFERENCES

- Babahosseini, H., Meghdari, A., Khorsand, M. and Alasty, A., 2009. "Optimal sliding mode control of AFM tip vibration and position during manipulation of a nanoscape". In *Proceedings of the ASME 2009 International Mechanical Engineering Congress and Exposition*. pp. 1–10.
- Balthazar, J.M., Tusset, A.M. and Bueno, A.M., 2012. "On control strategies, including parametric errors, applied to an Atomic Force Microscope nonlinear vibrating problem". In *1st International Symposium on Uncertainty Quantification and Stochastic Modeling (Uncertainties 2012)*. Maresias, SP.
- Binnig, G., Quate, C.F. and Gerber, C., 1986. "Atomic Force Microscope". *Physics Review Letters*, Vol. 56, pp. 930–933.
- Dankowicz, H., 2006. "Nonlinear dynamics as an essential tool for non-destructive characterization of soft nanostructures using tapping-mode atomic force microscopy." *Philosophical transactions. Series A, Mathematical, physical, and engineering sciences*, Vol. 364, No. 1849, pp. 3505–20.
- Fang, Y., Feemster, M.G., Dawson, D.M. and Jalili, N., 2002a. "Active Interaction Force Identification for Atomic Force Microscope Applications". , No. December, pp. 3678–3683.
- Fang, Y., Feemster, M.G., Dawson, D.M. and Jalili, N., 2002b. "Nonlinear Control Techniques for the Atomic Force Microscope System". *Dynamic Systems and Control*, Vol. 2002, pp. 373–380.
- Howard-Knight, J.P. and Hobbs, J.K., 2011. "Finite element modeling of atomic force microscopy cantilever dynamics during video rate imaging". *Journal of Applied Physics*, Vol. 109, No. 7, p. 074309.
- Israelachvili, J.N., 1991. *Intermolecular and Surface Forces*. Academic Press, 2nd edition.
- Jalili, N. and Laxminarayana, K., 2004. "A review of atomic force microscopy imaging systems: application to molecular metrology and biological sciences". *Mechatronics*, Vol. 14, No. 8, pp. 907–945.
- Meyer, E., 1992. "Atomic force microscopy". *Progress in Surface Science*, Vol. 41, No. 1, pp. 3–49.
- Misra, S., Dankowicz, H. and Paul, M.R., 2008. "Event-driven feedback tracking and control of tapping-mode atomic force microscopy". *Proceedings of the Royal Society A: Mathematical, Physical and Engineering Sciences*, Vol. 464, No. 2096, pp. 2113–2133.
- Nozaki, R., Balthazar, J.M. and Tusset, A.M., 2010. "Optimal linear control to an atomic force microscope (afm) problem with chaotic behavior". In *Proceedings of 9th Brazilian Conference of Dynamics and Their Applications (DINCON)*. Serra Negra, SP, pp. 371–377.
- Rodrigues, K.S., Balthazar, J.M., Tusset, A.M. and Pontes Jr., B.R., 2011. "Dynamical study of a piecewise-smooth model in tapping mode atomic force microscope". In *Proceedings of 10th Brazilian Conference of Dynamics and Their Applications (DINCON)*. Aguas de Lindoia, SP.
- Rutzel, S., Lee, S.I. and Raman, A., 2003. "Nonlinear dynamics of atomic-force-microscope probes driven in Lennard-Jones potentials". *Proceedings of the Royal Society A: Mathematical, Physical and Engineering Sciences*, Vol. 459, No. 2036, pp. 1925–1948.
- Stark, R., Schitter, G., Stark, M., Guckenberger, R. and Stemmer, A., 2004. "State-space model of freely vibrating and surface-coupled cantilever dynamics in atomic force microscopy". *Physical Review B*, Vol. 69, No. 8, pp. 1–9.
- Zhao, X. and Dankowicz, H., 2006. "Characterization of intermittent contact in tapping-mode atomic force microscopy". *Journal of Computational and Nonlinear Dynamics*, Vol. 1, No. 2, pp. 109–115.

8. RESPONSIBILITY NOTICE

The authors are the only responsible for the printed material included in this paper.